

IMPROVED FUSION PLASMA PERFORMANCE IN FUSION DEVICES ENABLED BY A NEW IMPURITY POWDER INJECTION SYSTEM

R. MAINGI, A. BORTOLON, E.P. GILSON, R. LUNSFORD, A. NAGY, Z. SUN, A. DIALLO, D.K. MANSFIELD

Princeton Plasma Physics Laboratory

Princeton, NJ USA

Email: rmaingi@pppl.gov

J.S. HU, X.Z. GONG, W. XU, L. ZHANG

Institute of Plasma Physics, Chinese Academy of Sciences

Hefei, China

H.H. LEE, S.H. HONG, S.W. YOON

Korea Institute of Fusion Energy

Daejeon, South Korea

Abstract

Low-Z impurities have been injected into a number of devices to improve performance, enabled by a relatively new apparatus that is designed to inject a wide range of impurity powders and granules. This paper summarizes the technical aspects of the injector and onboard diagnostics, while focusing on new ELM control results from the EAST and KSTAR devices. The new impurity injector was developed over the last 4 years, and uses vertically-mounted piezoelectric crystals for a horizontal drive off the edge of a surface into a drop tube. This apparatus can inject many different impurity species and particulate sizes. The lateral back-and-forth motion of up to 10 mm allows reproducible and calibratable impurity injection rates. An accelerometer and an optical sensor measure the injection rates. Boron powder injected with the system described above eliminated ELMs in EAST, while also modestly increasing stored energy and confinement and destabilizing an edge-localized mode with multiple harmonics. To assess the applicability of this technique to future devices (e.g. material inventory control requirements), the dependence of the minimum impurity injection rate for ELM elimination was measured as a function of heating power in EAST. The minimum injection rate tripled as the heating power was doubled, which is qualitatively consistent with more efficient screening by the scrape-off layer with increasing edge temperature and density. In KSTAR, both boron and boron nitride powder injection reduced the ELM frequency and created periods of ELM quiescence, while maintaining plasma stored energy. There was no low frequency mode triggered via impurity injection, as was observed in EAST. Boron nitride powder reliably reduced divertor D_α emission, while boron powder did not. Taken together, recycling reduction does not appear to be a requirement to trigger ELM quiescent phases in KSTAR.

1. INTRODUCTION

Impurities are injected into magnetic fusion devices to improve plasma performance in at least three ways: enhanced power exhaust, wall conditioning, and edge pedestal and edge-localized mode (ELM) control. Each of these can have a beneficial effect on core impurity content and even global energy confinement. Historically impurities have been injected in gaseous form, which limits the breadth of compounds that can be injected. A new technology has been developed that enables injection of a wide range of solid impurities in microscopic (10-100 μm) and macroscopic ($> 100 \mu\text{m}$) particles [1]. These injections can be used in small quantities for either mildly perturbative diagnostic purposes, or in larger quantities to modify the boundary and even core plasma. This paper briefly describes the technical aspects of the injector and onboard diagnostics, and presents new results on ELM and recycling control from the EAST and KSTAR devices.

The first-generation impurity injector developed at the Princeton Plasma Physics Laboratory dropped spherical, metallic impurities, e.g., lithium, onto a vibrating piezoelectric disk driven at resonant frequencies; the impurities were accelerated via gravity through a hole in the center of the disk into a drop tube and into the boundary plasma [2]. This first-generation injector was used to eliminate ELMs in NSTX-U, similar to the observations with pre-discharge Li evaporation[3]. The new impurity powder dropper (IPD), developed over the last 4 years, uses vertically-mounted piezoelectric crystals for a horizontal drive off the edge of a surface into a drop tube (Figure 1), and is compatible with a wide range of impurity species and sizes. The lateral back-and-forth motion of up to 1 mm allows reproducible and calibratable impurity injection rates. An accelerometer and an optical sensor measure the injection rates, which are optimized in the 1-100 mg/s range optimal for low-Z impurities in present devices. This new dropper is also capable of injecting large particle sizes, e.g., nominal 700 μm diameter granules, into plasma discharges. The latest deployments feature four independent drop units using a common drop tube; weights have been added to each unit to achieve distinct resonant frequencies to minimize unintentional injection

of impurities from the other three units when only one unit is activated. Versions of these droppers have been implemented on the ASDEX-Upgrade [4, 5], DIII-D [6-8], EAST [9-11], KSTAR [12], and LHD [13] devices (injection geometries indicated in Figure 1), and a related concept was deployed on the W7-X device [14, 15]. A new IPD was recently installed [16] on the WEST device.

2. EXPERIMENTS IN EAST

EAST is typically operated in the 0.5 MA and 2.5 T range, aiming to achieve 400s long H-mode discharges with RF heating techniques and high-Z plasma-facing components (PFCs)[17] to prepare for the Chinese Fusion Engineering Test Reactor (CFETR). Current experiments have achieved 60-100s long H-mode discharges, in which Li wall conditioning played a significant enabling role [18, 19]. For science experiments, EAST has a complement of heating methods: neutral beam injection (NBI), lower hybrid heating and current drive (LHCD), electron cyclotron resonant heating (ECRH), and ion cyclotron radio frequency (ICRF). Previously Li powder injection into EAST suppressed ELMs when using the double-null divertor configuration with carbon PFCs, with normalized confinement ~ 0.75 relative to ITERH98y2 scaling[20]. Using Li powder to suppress Type-I ELMs was extended in recent years to upper-single null configuration using the W PFCs, with confinement ~ 1.1 relative to ITERH98y2 scaling[21]. However the Li powder injection results in reduced recycling and increased deuterium retention, which could have drawbacks for reactors unless flowing liquid metals PFCs are used to move and ultimately remove the retained deuterium/tritium compounds. Hence there is interest in using other low-Z compounds that do not directly reduce recycling and enhance retention.

On EAST, the IPD was installed in a vertical port that injects directly into the private flux region in upper single-null discharges. The drop tube has a ~ 4.5 m length, leading to gravitationally accelerated drop velocities of ~ 10 m/s. The IPD complements a classic Li powder dropper [2] that drops radially outboard into the scrape-off layer (SOL) – see Figure 1b. In the first set of experiments, three of the four IPD tubes were loaded with powders: $\sim 70\mu\text{m}$ B powder, $50\mu\text{m}$ Li powder, and $\sim 700\mu\text{m}$ Li granules. Weight was added to each IPD channel to avoid overlap in the resonant frequencies that can result in unintended drops from channels adjacent to the active channel. Note that the frequency overlap needs to be minimized over the entire range of reservoir inventory, because the channel mass decreases modestly as the reservoir is depleted with long term usage.

To compare with the Li powder injection results, B powder was injected into Type-I ELMy H-modes into the X-point region of an upper single-null diverted configuration using the tungsten PFCs, with ion grad-B drift toward the upper X-point [9, 10]. In these discharges the ELMs were completely eliminated when the B injection exceeded a threshold injection rate of several mg/s ($\sim 10^{20}$ B atoms/s). A modest ~ 5 - 10% increase in stored energy and energy confinement was also observed, likely due to the elimination of convective and conductive losses from the ELMs. Radiated power in the core and electron density were matched, and ELMs returned within 0.5 s after termination of B injection. Use of B powder injection to eliminate ELMs was very robust, achieved over a wide density range (2.5 - 7.5×10^{19} m^{-3} , 25-85% of the Greenwald density limit scaling), heating power range (2.8-7.5 MW), q_{95} range (4.4-7.2), in both directions of the toroidal magnetic field, and with either D or He majority ion species.

Figure 2 compares three discharges with auxiliary heating power of 3 MW, entirely from lower hybrid waves and ECRH. The reference no powder discharge (blue) has ELMs throughout. The discharge with a powder injection

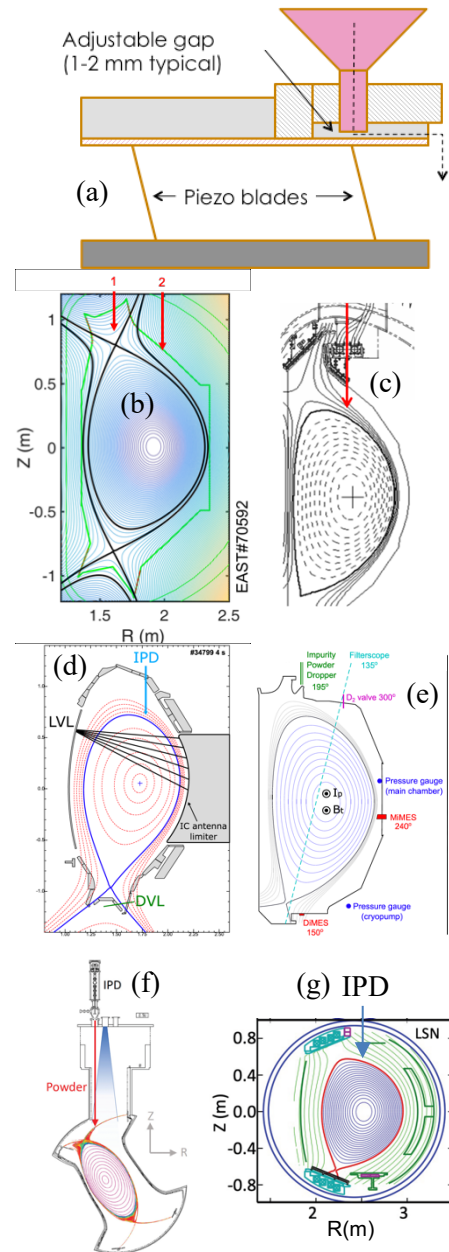


Figure 1: (a) schematic of impurity powder dropper (IPD) with horizontal vibration and powder motion. IPD injection location in (b) EAST, (c) KSTAR, (d) ASDEX-Upgrade, (e) DIII-D, (f) LHD and (g) WEST.

rate at 2.5 mg/s (1.4×10^{20} B atom/s, green curves) resulted in complete ELM elimination, while the discharge with a powder injection rate at 2 mg/s (1.1×10^{20} B atom/s, orange curves) resulted in ELM mitigation. ELMs were suppressed or mitigated by 5.1s in the two discharges with B injection. The B injection initiation timing corresponds to the rise of the B_v signal relative to the reference no-B discharge at ~ 4.7 s (panel (b)), and in both cases, B injection is terminated at ~ 6.7 s, resulting in the eventual resumption of ELM activity. The upper divertor D_α emission in panel (c) shows a decrease relative to the ELMy H-mode no-B reference *only after* ELM activity ceases; this is confirmed by detailed timing scans [11]. This observation suggests that a substantial fraction of the divertor recycling flux originates from ELM plasma expulsions impinging on the PFCs. In subsequent experiments with accumulated B dose, B powder was observed to reduce divertor D_α emission before ELM suppression, but this result from the first B injection of the campaign means that *a reduction in recycling flux is not required for ELM suppression*.

ELM elimination with powder injection above the threshold injection rate was correlated with the appearance of a ~ 2 -5 kHz edge coherent mode. This mode can be seen on multiple diagnostics that span the boundary region: AXUV diodes that measure radiated power, divertor D_α emission, tile-embedded divertor Langmuir probes at the inner and outer strike points, line-integrated background D_α along He BES system, electron cyclotron emission (ECE), and Mirnovs at all poloidal locations[22]. The fundamental and dominant toroidal mode number is $n=1$, and the mode peaks marginally inside the foot of the H-mode pedestal, spanning just inside and outside the separatrix. The mode can be seen from the displayed FFT of an AXUV diode signal near the upper X-point, shown in panels 2(d)-(f). The reference ELMy no-B powder discharge shows no mode, while both of the discharges with powder injection show the mode with several harmonics. Note that in #93153, the mode onset can be observed before B powder injection. While mode onset before B injection is atypical, the use of B powder injection uniformly increases the apparent intensity of the mode in those discharges, signifying that B injection can intensify an existing mode.

To assess the applicability of this technique to future devices (e.g. material inventory control requirements), the dependence of the threshold impurity injection rate for ELM elimination on heating power is important. This threshold rate was measured as a function of heating power between 3 and 6 MW at $I_p=0.5$ MA and $B_t=2.5$ T. The highest power discharges investigated for which the ELM suppression threshold was measured in this experiment are displayed in Figure 3. These discharges had ~ 3 MW of LHCD + ECH, supplemented by 3 MW of co-directed NBI. The reference no powder discharge (blue) had ELMs throughout. The discharge with powder injection rate at 8 mg/s (4.4×10^{20} B atom/s, green curves) results in complete ELM elimination, while the discharge with powder injection rate at 6 mg/s (3.3×10^{20} B atom/s, orange curves) results in ELM mitigation. ELMs are suppressed or mitigated by ~ 5 s in the two discharges with B injection, i.e. the timing is similar to the ELM control timing for the lower power discharges in Figure 2. The B injection initiation time corresponds to the rise of the B_v signal relative to the reference no-B discharge at ~ 4.5 s (panel (b)), and in both cases, B injection is continued through NBI ramp down. The upper divertor D_α emission in panel (d) shows a decrease relative to the ELMy H-mode no-B reference only after ELM activity ceases, confirming the importance of ELMs in setting the baseline value, as also observed in the lower power discharges.

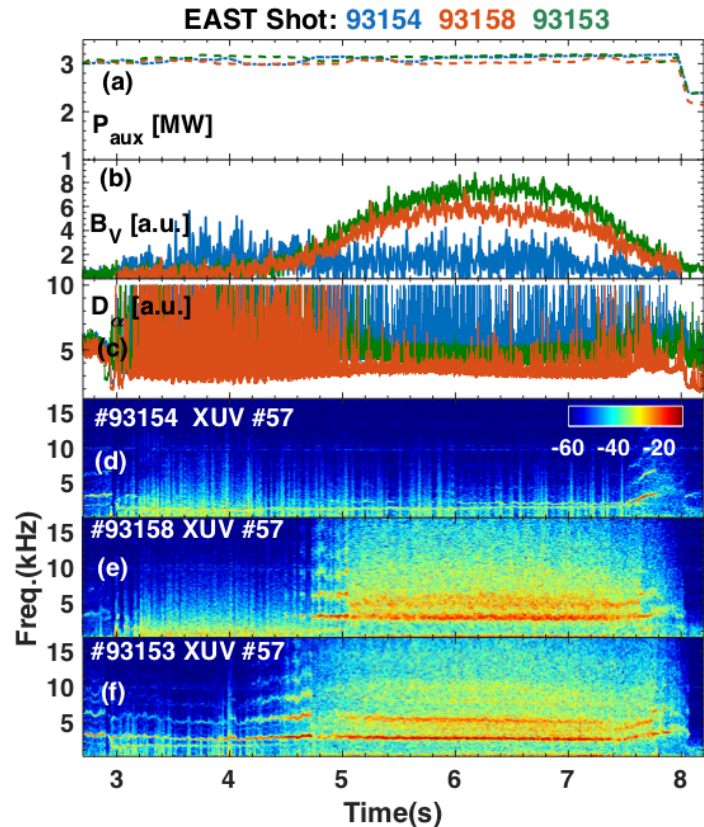


Figure 2: comparison of three discharges with different B powder injection rates at low heating power in EAST: (a) heating power P_{aux} , (b) B_v edge emission, (c) Upper divertor D_α emission, (d)-(f) spectrogram from AXUV diode channel #57 for each discharge. ELM elimination in green (mitigation in orange) is obtained at the higher (lower) B injection rate, with the no-B injection reference discharge in blue.

A mode destabilized during powder injection can be seen from the displayed FFT of an AXUV diode signal near the upper X-point, shown in panels 3(d)-(f), i.e. the same channel used in panels 2(d)-(f). The reference ELMy no-B powder discharge shows no mode, while both of the discharges with powder injection show the mode with multiple harmonics. Note that in #93165 and #93168, the mode onset can be observed only after B powder injection, but before the ELMs have been eliminated. Note that both of these discharges also show a lower frequency mode at ~ 3 kHz than the multi-harmonic mode correlated with ELM suppression (fundamental at 4 kHz). In #93165 the lower frequency mode disappeared at ~ 5.2 s, while it persisted, albeit intermittently, in #93166. This second lower frequency mode is unrelated to ELM elimination as it is not a common observation in our experiments.

The threshold B flow rate for ELM suppression was also measured at an intermediate power level of ~ 5 MW. Figure 4 shows all three datasets. It can be seen that the minimum B injection rate for ELM suppression tripled as the heating power was doubled. This observation is qualitatively consistent with more efficient screening by the SOL with increasing edge temperature and density, as expected when the heating power is increased.

Current research is focused on identifying the mode destabilized by powder injection, and its possible drive mechanisms. Modeling of the data with the XGC code has suggested that the fluctuation is related to a geodesic acoustic mode (GAM), whose eigenfunction peaks at the X-point [23]. This could explain why the mode is so easy to trigger with the injection geometry at EAST, and why it hasn't been clearly observed at other devices where the IPD has been deployed.

3. EXPERIMENTS IN KSTAR

The KSTAR device [24] targets long pulse H-mode discharge development, with a focus on the use of resonant magnetic perturbations to suppress ELMs [25], in preparation for a demonstration reactor, K-DEMO. ELMy H-modes with durations > 60 s have been obtained with neutral beam heating and discharge tailoring, using all carbon PFCs at present. In KSTAR ELMy H-modes, both B and BN powders were injected with the IPD, using either discrete drops spaced several seconds apart, or continuous drops[12].

Both B and BN powder injection triggered ELM-stable phases of several seconds duration while maintaining good confinement. These discharges were run with $I_p = 0.5$ MA, $B_t = 1.8$ T, in lower single-null configuration with ion grad-B drift toward the lower X-point, and 1.5 MW of NBI heating. Characteristics of representative discharges are compared in Figure 5. Each column of panels shows divertor D_α emission, radiated power P_{rad} , stored energy W_{MHD} , the IPD powder-monitoring photodiode signal, the IPD flow meter reading, and the NBI power P_{NBI} . Four discharges are shown: panels (a) is a reference ELMy H-mode with no powder injection. Panels (b) has B powder injection in two discrete drops at about $t=10$ s and $t=15$ s at rates of 5 mg/s for 0.5 s each (2.7×10^{20} B atoms/s).

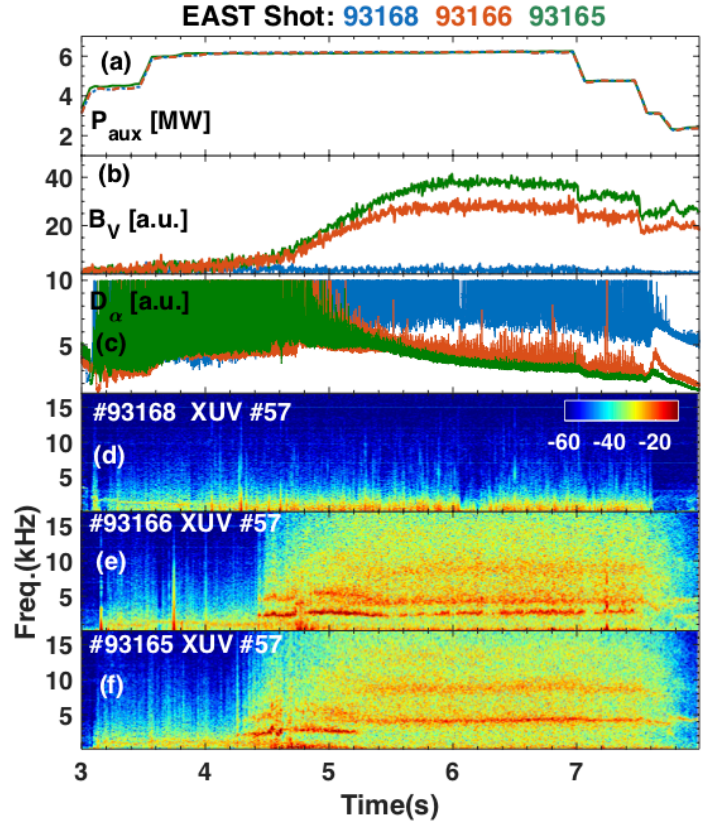


Figure 3: comparison of three discharges with different B powder injection rates at high heating power in EAST: (a) heating power P_{aux} , (b) B_V edge emission, (c) Upper divertor D_α emission, (d)-(f) spectrogram from AXUV diode channel #57 for each discharge. ELM elimination in green (mitigation in orange) is obtained at the higher (lower) B injection rate, with the no-B injection reference discharge in blue.

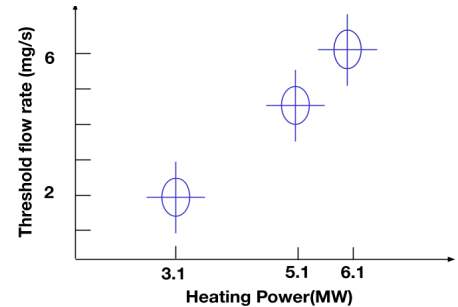


Figure 4: dependence of threshold B flow rate for ELM suppression as a function of auxiliary heating power in EAST, with ion grad-B drift toward the upper X-point. Note the suppressed 0 on the x-axis.

Panels (c) show BN powder injection in three discrete drops at 25 mg/s (6×10^{21} B and N atoms/s) at $t=2$, $t=6$, and $t=11$ s, with each drop programmed for 0.1 s. Panels (d) show BN powder injection in a continuous at 2.5 mg/s (6×10^{20} B and N atoms/s).

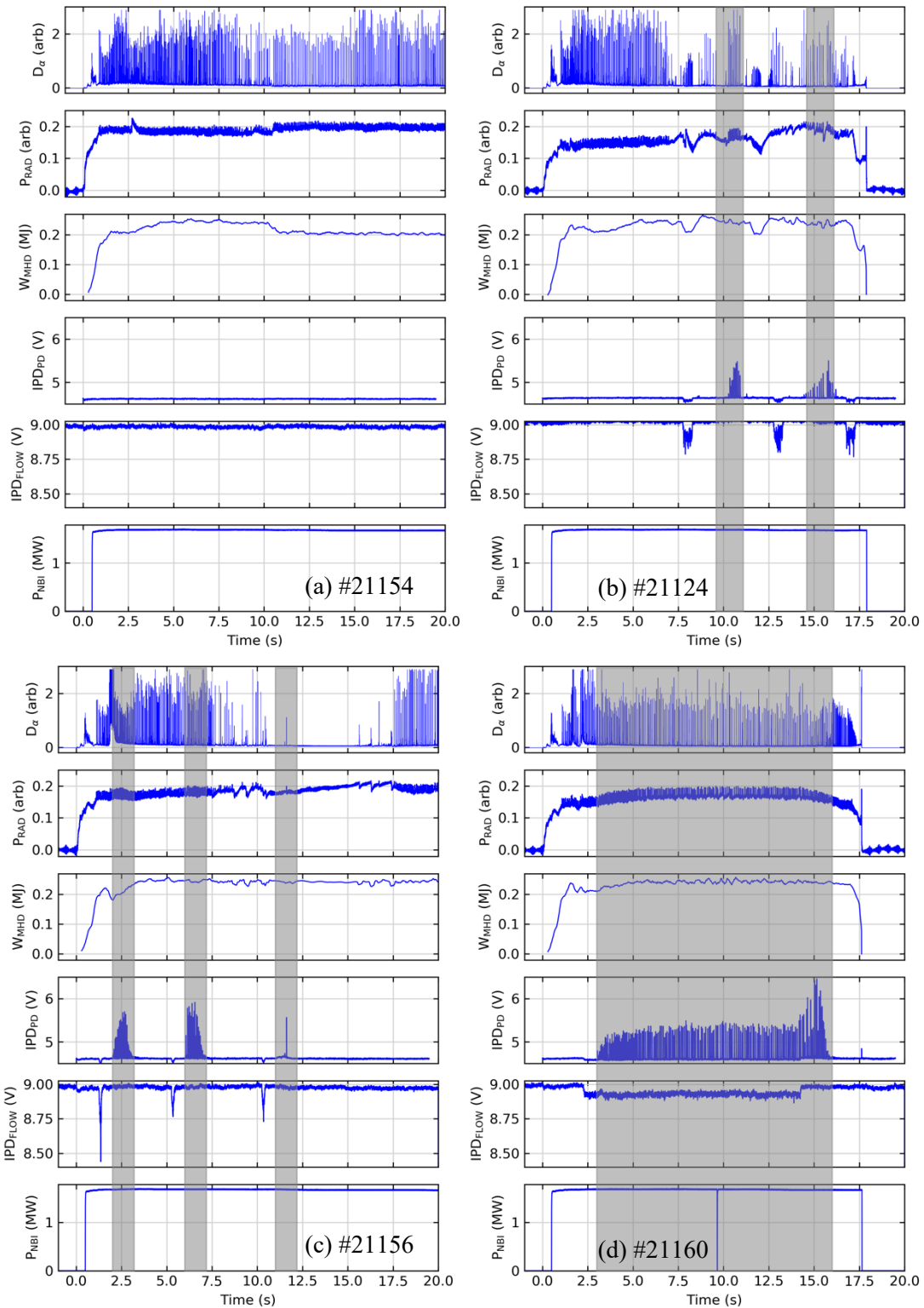


Figure 5: Comparison of four discharges in KSTAR: reference no powder ELMy H-mode in panels (a), B powder injection in panels (b), BN powder at high rate in panels (c), and BN powder at low rate, continuous in panels (d). The shaded regions indicate B injection timing after falling through the drop tube and impacting the plasma.

The reference discharge in panels 5(a) had ELM frequency of 40-50 Hz from about $t=2-7$ s. The ELM frequency naturally slowed down by 30% at about $t=8$ s, while the stored energy decreased by 10-15%. This observed reduction in ELM frequency is not uncommon in 20 s long KSTAR H-modes, and is attributed to slow evolution of the boundary shape and strike points, along with temperature rise of the PFCs.

In this first KSTAR experiment with B powder injection, B was injected in six discharges with the IPD at rates between 3.5 and 10 mg/s ($2.0-5.6 \times 10^{20}$ B atom/s), with periodically intermingled reference no-B discharges. Panels 5(b) shows a discharge with 2 B injection pulses at 5 mg/s (2.8×10^{20} B atom/s) for 0.5 s durations. Prior to this discharge, 30 mg of B powder had cumulatively been injected in five discharges. The ELM frequency and size (based on D_α intensity spikes) were both reduced, starting at $t \sim 7$ s. In contrast to the no-B reference discharge, stored energy was maintained except for a couple of transient phases. Two intermediate discharges (#21117 and #21118) between this one and the morning reference discharge, #21107, also showed periods of ELM quiescence.

In the first KSTAR experiment with BN powder injection, BN was injected in three pulses with the IPD at rates between 2.5 and 25 mg/s ($0.6-6.0 \times 10^{21}$ B and N atom/s). Panels 5(c) shows a discharge with 2 B injection pulses at 25 mg/s (6×10^{21} B and N atoms/s) for 0.1 s durations. Here a dramatic change in ELM frequency was observed following the second BN pulse, including a ~ 5 s long ELM quiescent phase. Stored energy was maintained throughout the discharge. Panels 5(d) shows a discharge with continuous BN injection at 2.5 mg/s (6×10^{20} B and N atoms/s) from $t=3-16$ s. A drop in ELM frequency (up to 50%) and ELM size was observed, indicating that this injection rate was insufficient to trigger ELM quiescence. We note while the triggered ELM quiescent phases with BN injection were tantalizing, the results could not be reproduced in subsequent experiments in 2019, leading the analysis to focus on recycling reduction and wall conditioning effects [12]. We also note that no low frequency edge harmonic mode was destabilized in KSTAR, as was seen on EAST.

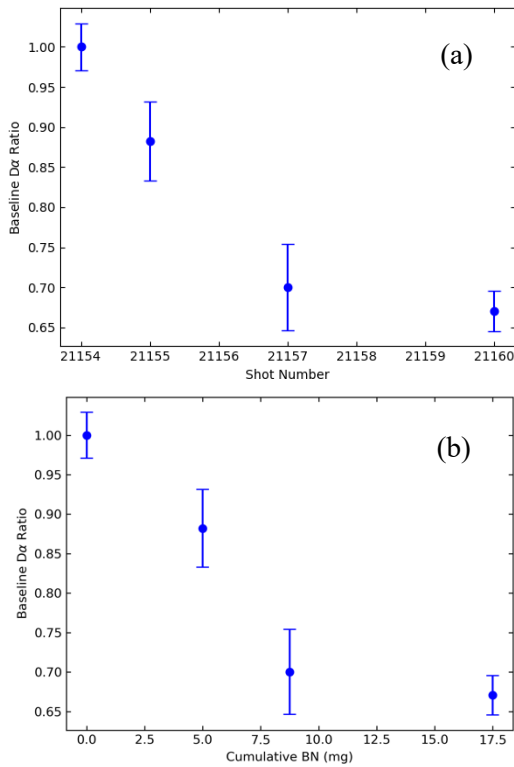


Figure 6: D_α baseline signal relative to reference no powder discharge in KSTAR for 25 mg/s BN bursts (#21155), 12.5 mg/s BN bursts (#21157), and 2.5 mg/s continuous drop (#21160). Panel (a) plots the ratio as a function of discharge number, and panel (b) vs. cumulative BN drop.

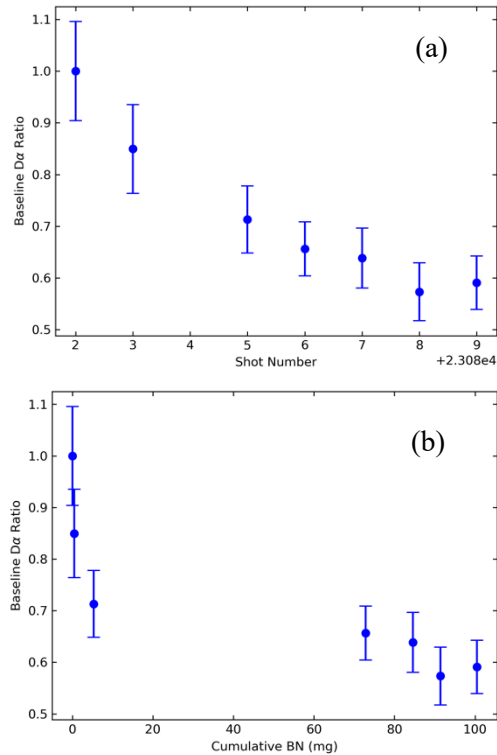


Figure 7: D_α baseline signal relative to reference no powder discharge in KSTAR from 2019 experiments with BN injection. Panel (a) plots the ratio as a function of discharge number, and panel (b) vs. cumulative BN drop.

Turning first to the BN experiments, inspection of the D_α emission baseline shows a marked reduction of the recycling flux with BN injection as compared with the reference discharge. Figure 6 quantifies this reduction as a function of discharge number and cumulative BN injection. A $\sim 33\%$ reduction is observed, which appears to saturate at the lowest BN injection rate in #21160. In the 2019 BN injection experiment, a similar reduction in D_α

emission baseline was observed, up to 40%, as the cumulative amount was increased from 17.5 mg in 2018 to 100 mg in 2019 (Figure 7). These two datasets indicate that the recycling reduction is either not an integral part of triggering ELM quiescent phases, or is a necessary but insufficient criterion to ensure ELM quiescence.

Turning back to the B powder injection experiment, Figure 8 plots the D_α emission baseline relative to the reference no-B powder discharge as a function of discharge number and cumulative B injection. No obvious effect on recycling (as measured by baseline D_α emission) was observed; we conjecture that the lack of impact on recycling is due to low accumulated B dose. This further suggests that recycling changes do not play a dominant role in the triggering of Elm quiescent phases in KSTAR. Other explanations being considered for the triggered ELM quiescence include increase in edge Z_{eff} leading to reduced bootstrap current and/or increase in low-Z edge impurity content leading to deuterium dilution and a reduction of the ion pressure gradient, both of which provide improved stability to peeling-ballooning modes.

4. SUMMARY AND CONCLUSIONS

The impurity powder dropper has enabled a wide range of new experimental studies on a number of international devices. Table 1 summarizes the impurity species used in each device from the listed references, and whether a positive result was obtained in the area of wall conditioning, power exhaust, or ELM control.

In this paper we have summarized new results on ELM control in EAST and KSTAR. In EAST B powder injection into the upper X-point region reliably eliminates ELMs over a wide operational window. A low frequency near-separatrix edge-localized fluctuation is correlated with ELM suppression and B powder injection. We have measured for the first time the threshold B injection rate to suppress ELMs, and find that it increases with auxiliary heating power, as qualitatively expected from increased SOL screening in high power discharges. Additional modelling in the Diallo et al. companion IAEA paper has indicated the importance of injection into the X-point region, suggesting new experiments on EAST to compare low-field side SOL B powder injection with X-point injection, as well as comparing C and B_4C powder injection to B powder. Modelling of the ablation and separatrix penetration is needed to project minimum injection thresholds for future devices, in which material inventory management will become a central issue.

In KSTAR we have demonstrated that both B and BN powder can trigger phases of ELM quiescence of several seconds, with BN having the larger impact. BN injection also reduces baseline D_α emission, while B injection does not. Taken together these results suggest that recycling control is not central to the stabilization of ELMs with powder injection in KSTAR. Alternate explanations for triggering of ELM quiescent phases, related to Z_{eff} increase and/or deuterium ion dilution, are being considered.

ACKNOWLEDGEMENTS

U.S. authors of this research were supported by the U.S. Dept. of Energy Contract DE-AC02-09CH11466. Chinese authors were supported by the National Key Research and Development Program of China (2017YFA0402500 and 2017YFE0301100), and the National Nature Science Foundation of China (11625524, 11775261, 11605246). Korean authors were supported by the Ministry of Science and ICT of the Republic of Korea through the Korean ITER Technology R&D Program (IN2010-3) and KSTAR Program (EN2001-11), and by the National R&D Program through the National Research Foundation of Korea (NRF), funded by the Ministry

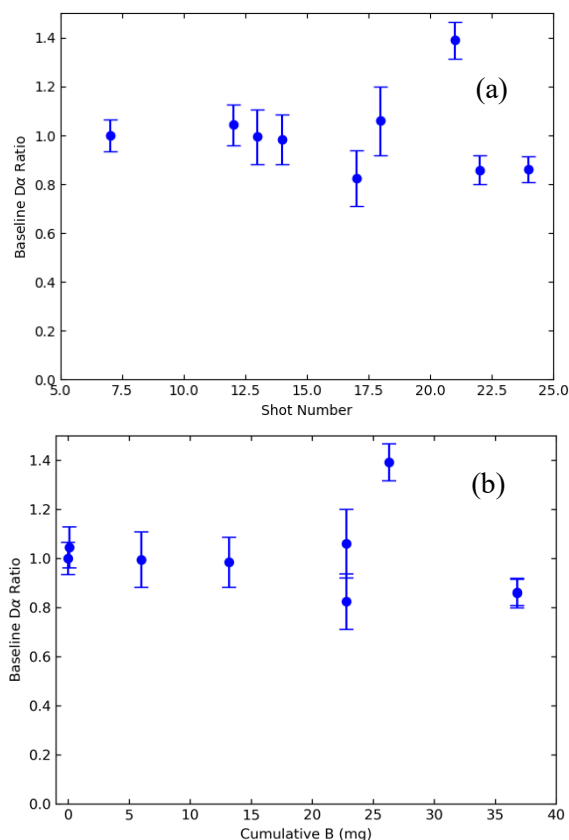


Figure 8: D_α baseline signal relative to reference no-B powder discharge in KSTAR experiments as a function of (a) discharge number from sequence #21107-#21124. The discharge number is obtained by adding 21000 to the x-axis value. Panel (b) plots the data vs cumulative B injection.

of Science and ICT (NRF-2019M1A7A1A03087560). We gratefully acknowledge the contributions from the EAST and KSTAR technical staff. The United States Government retains a non-exclusive, paid-up, irrevocable, world-wide license to publish or reproduce the published form of this manuscript, or allow others to do so, for United States Government purposes.

Table 1: Devices using the IPD and successful experiments in three main areas described in the manuscript. The NSTX results used a Lithium powder dropper, a predecessor to the IPD, as described in the manuscript.

Device	Impurities used in IPD	Wall Conditioning e.g. D_{α} reduction	Power exhaust enhanced	ELMs mitigated or pedestal improved or τ_E increased
EAST	B powder	√	√	√
	Li powder	√		√
	Li granules (0.7mm)	√		√
KSTAR	B powder	√		√
	BN powder			√
DIII-D	B powder	√	√	√
	BN powder	√		
	Li powder			
ASDEX-Upgrade	B powder	√	√	√
	BN powder	√		
LHD	B powder	√		√
WEST	B powder	In progress		
NSTX* (LiPD)	Li powder	√		√
W7-X** (probe mounted injector)	B ₄ C powder			√

REFERENCES

1. A. Nagy *et al.*, 2018 *Rev. Sci. Instrum.* **89** 10K121
2. D. K. Mansfield *et al.*, 2010 *Fusion Eng. Des.* **85** 890
3. D. K. Mansfield *et al.*, 2009 *J. Nucl. Mater.* **390-391** 764
4. A. Bortolon *et al.*, 2019 *Nucl. Mater. Energy* **19** 384
5. R. Lunsford *et al.*, 2019 *Nucl. Fusion* **59** 126034
6. A. Bortolon *et al.*, 2020 *Nucl. Fusion* **60** 126010
7. F. Effenberg *et al.*, 2021 *Proc. 28th International Conf. on Fusion Energy, 10-15 May 2021*
8. R. Lunsford *et al.*, 2021 *Proc. 28th International Conf. on Fusion Energy, 10-15 May 2021*
9. Z. Sun *et al.*, 2021 *Nucl. Fusion* **61** 014002
10. R. Maingi *et al.*, 2020 *J. Fusion Energy* **39** 429
11. Z. Sun *et al.*, 2021 *Nucl. Fusion* **61** subm.
12. E. P. Gilson *et al.*, 2021 *Nucl. Mater. Energy* subm.
13. F. Nespoli *et al.*, 2020 *Nuclear Materials and Energy* **25** 100842
14. A. Nagy *et al.*, 2019 *Fusion Eng. Des.* **146** 1403
15. R. Lunsford *et al.*, 2021 *Phys. Plasmas* **28** subm.
16. G. Bodner *et al.*, 2021 *Proc. 2021 Euro. Conf. on Contr. Fusion and Plasma Physics, 21-25 June 2021.*
17. B. Wan *et al.*, 2015 *Nucl. Fusion* **55** 104015
18. X. Gong *et al.*, 2017 *Plasma Science and Technology* **19** 032001
19. Z. Sun *et al.*, 2019 *Nucl. Mater. Energy* **19** 124
20. J. S. Hu *et al.*, 2015 *Phys. Rev. Lett.* **114** 055001
21. R. Maingi *et al.*, 2018 *Nucl. Fusion* **58** 024003
22. Z. Sun *et al.*, 2021 *Phys. Plasmas* **28** in prep.
23. A. Diallo *et al.*, 2021 *Proc. 28th International Conf. on Fusion Energy, 10-15 May 2021*
24. G. S. Lee *et al.*, 2001 *Nucl. Fusion* **41** 1515
25. Y. Jeon *et al.*, 2012 *Phys. Rev. Lett.* **109** 035004